

1 TERRIGENOUS MATERIAL SUPPLY TO THE PERUVIAN CENTRAL CONTINENTAL
2 SHELF (PISCO 14°S) DURING THE LAST 1000 yr: PALEOCLIMATIC IMPLICATIONS.

3 F. Briceño-Zuluaga^{1,2}, A. Sifeddine^{1,2,3}, S. Caquineau^{2,3}, J. Cardich^{1,2}, R. Salvattei⁵, D.
4 Gutierrez^{2,4}, L. Ortlieb^{2,3}, F. Velazco^{2,4}, H. Boucher^{2,3}, C. Machado^{1,2}.

5

6 ¹ Departamento de Geoquímica, Universidade Federal Fluminense - UFF, Niterói, RJ – Brasil.

7 ² LMI PALEOTRACES (IRD-France, UPMC-France, UA-Chile, UFF-Brazil, UPCH-Peru).

8 ³ IRD-Sorbonne Universités (UPMC, CNRS-MNHN), LOCEAN, IRD France-Nord, Bondy,
9 France.

10 ⁴ Instituto del Mar del Peru IMARPE. Esquina Gamarra y General Valle s/n, Callao 22000, Peru

11 ⁵ Institute of Geoscience, Kiel University, Germany.

12

13 Correspondence to: franciscojavier@id.uff.br

14 **Abstract**

15 In the Eastern Pacific, lithogenic input to the ocean responds to variations of the atmospheric
16 and oceanic system and their teleconnections over different timescales. Atmospheric (e.g., wind
17 fields), hydrological (e.g., fresh water plumes) and oceanic (e.g., currents) conditions determine
18 the transport mode and the amount of lithogenic material transported from the continent to the
19 continental shelf. Here, we present the grain size distribution of a composite record of two
20 laminated sediment cores retrieved from the Peruvian continental shelf that record the last
21 ~1000 yr at a sub-decadal to centennial time-series resolution. We propose novel grain-size
22 indicators of wind intensity and fluvial input that allow reconstructing the oceanic-atmospheric
23 variability modulated by sub-decadal to centennial changes in climatic conditions. Four grain
24 size modes were identified. Two are linked to aeolian inputs (M3: ~54 μm and M4: ~91 μm on
25 average), the third is interpreted as a marker of sediment discharge (M2: ~10 μm on average),
26 and the last is without an associated origin (M1: ~3 μm). The coarsest components (M3 and
27 M4) dominated during the Medieval Climate Anomaly (MCA) and the Current Warm Period
28 (CWP) periods, suggesting that aeolian transport increased as consequence of surface wind
29 stress intensification. In contrast, M2 displays an opposite behavior, exhibiting an increase in
30 fluvial terrigenous input during the Little Ice Age (LIA) in response to more humid conditions
31 associated with El Niño like conditions. Comparison with other South American paleoclimate
32 records indicates that the observed changes are driven by interactions between meridional
33 displacement of the Intertropical Convergence Zone (ITCZ), the South Pacific Sub-tropical
34 High (SPSH) and Walker Circulation at decadal and centennial time scales.

35

37 The Pisco region (~14-15°S) hosts one of the most intense coastal upwelling cells off Peru due
38 to the magnitude and persistence of alongshore equatorward winds during the annual cycle (Fig.
39 1B). Regional winds can also be affected at interannual timescales by El Niño Southern
40 Oscillation (ENSO) variability (i.e., enhanced or weakened during La Niña and El Niño events,
41 respectively), as well as by the Pacific Decadal Oscillation (PDO) at decadal timescales (Flores-
42 Aqueveque et al., 2015). These factors also affect the inputs of terrigenous material to the
43 Peruvian continental shelf. Saukel et al. (2011) found that wind is the major transport agent of
44 terrigenous material west of the Peru–Chile Trench between 5°S and 25°S. Flores-Aqueveque et
45 al. (2012) showed that in the arid region of northern Chile, transport of aeolian coarser particles
46 (approximately ~100 μm) is directly related to interannual variations in the domain of the
47 strongest winds. The Pisco region is also home to local dust storms called “Paracas”, which
48 transport dust material to the continental shelf as a response to seasonal erosion and transport
49 events in the Ica desert (~15°S). This process reflects atmospheric stability conditions and
50 coastal sea surface temperature connections (Gay, 2005). In contrast, sediment fluvial discharge
51 is more important on the northern coast of Peru where there are large rivers, and it decreases
52 southward where arid conditions are dominant (Garreaud and Falvey, 2009; Scheidegger and
53 Krissek, 1982). This discharged material is redistributed southward by coastal currents along the
54 continental shelf (Montes et al., 2010; Smith, 1983). In addition, small rivers exist in our study
55 area, such as the Pisco River, which can increase their flow during strong El Niño events
56 (Bekaddour et al., 2014). It has also been demonstrated that during El Niño events and
57 coincident positive PDO, there is an increase in precipitation along northern Peru and,
58 consequently, higher river discharge, mainly from the large rivers (e.g., the Santa River),
59 whereas an opposite behavior is observed during La Niña events and negative phase of PDO
60 (Bekaddour et al., 2014; Böning and Brumsack, 2004; Lavado Casimiro et al., 2012; Ortlieb,
61 2000; Rein, 2005, 2007; Scheidegger and Krissek, 1982; Sears, 1954).

62

63 Grain size distributions in marine sediments may indicate different sources and/or depositional
64 processes that can be expressed as polymodal distributions (e.g., Pichevin et al., 2005; Saukel et
65 al., 2011; Stuut and Lamy, 2004; Stuut et al., 2002, 2007; Sun et al., 2002; Weltje and Prins,
66 2003, 2007). The polymodal distribution makes the classification of grain size composition an
67 essential step in identifying the different sedimentary processes and the past environmental
68 conditions behind them (e.g., climate, atmosphere and ocean circulation) (Bloemsma et al.,
69 2012; Flores-Aqueveque et al., 2012, 2015; Pichevin et al., 2005; Ratmeyer et al., 1999; Saukel
70 et al., 2011; Stuut et al., 2005, 2007; Sun et al., 2002). The grain-size distributions of lithogenic
71 materials in marine sediments can thus be used to infer relative wind strengths and aridity on the

72 assumption that more vigorous atmospheric circulation will transport coarser particles to a
73 greater distance and that the relative abundance of fluvial particles reflects precipitation patterns
74 (e.g., Hesse and McTainsh, 1999; Parkin and Shackleton, 1973; Pichevin et al., 2005; Stuut and
75 Lamy, 2004; Stuut et al., 2002).

76 A significant number of studies have described the climatic, hydrologic and oceanographic
77 changes during the last 1000 years on the Peruvian continental shelf (Ehlert et al., 2015;
78 Gutiérrez et al., 2011; Salvattecí et al., 2014b; Sifeddine et al., 2008). Evidences of changes in
79 the Humboldt Current circulation system and in the precipitation pattern have been reported.
80 Salvattecí et al., (2014b) show that the Medieval Climatic Anomaly (MCA) exhibits two distinct
81 patterns of Peruvian upwelling characterized by weak/intense marine productivity and sub-
82 surface oxygenation, respectively, as a response to the intensity of SPSH linked to the Walker
83 circulation. During the Little Ice Age (LIA), an increased sediment discharge over the Pisco
84 continental shelf was described, as well as a stronger oxygenation and lower productivity
85 (Gutiérrez et al., 2009; Salvattecí et al., 2014b; Sifeddine et al., 2008). In addition, during the
86 Current Warm Period (CWP), the PUE exhibited 1) an intense Oxygen Minimum Zone (OMZ)
87 and an increase in marine productivity, 2) a significant SST cooling ($\sim 0.3\text{--}0.4^\circ\text{C decade}^{-1}$), and
88 3) an increase in terrigenous material input (Gutiérrez et al., 2011).

89 Here we present new data regarding the effective mode of transport of mineral fractions to the
90 Pisco shelf during the last millennium, confirming previous work and bringing new highlights
91 about the climatic mechanism behind Humboldt circulation and atmospheric changes, especially
92 during the MCA. Our results identify wind intensification during the second part of the MCA
93 and CWP, in contrast to a decrease of the wind intensity during the LIA and the first part of the
94 MCA synchronous with fluvial discharge increases. Comparisons with other paleoclimate
95 records indicate that the ITCZ displacement, the SPSH and the Walker circulation were the
96 main drivers for the hydroclimate changes along the coastal Peruvian shelf during the last
97 millennium.

98 **2. Sedimentary settings.**

99 Reinhardt et al., (2002); Suess et al., (1987) and Gutierrez et al., (2006) described the
100 sedimentary facies in the Peruvian shelf and the role of currents in the erosion process as well as
101 the redistribution and favorable hemipelagic sedimentation of material over the continental
102 shelf. These studies showed that high resolution sediment records are present in specific
103 localities of the Peruvian continental margin. Suess et al., (1987) described the two sedimentary
104 characteristic facies between $6 - 10^\circ\text{S}$ and between $11 - 16^\circ\text{S}$. The first one, $6 - 10^\circ\text{S}$
105 (Salaverry Basin), is characterized by the absence of hemipelagic sediment accumulation
106 because in this zone the southward poleward undercurrent is strong. The second one, $11 - 16^\circ\text{S}$

107 Lima Basin, is characterized by a lens shaped depositional center of organic-rich mud facies
108 favored by oceanographic dynamics from the position and low velocity of the southward
109 poleward current on the continental shelf (Reinhardt et al., 2002; Suess et al., 1987). High-
110 resolution sediment echo sounder profiles further characterize the mud lens nature and
111 complement the continental shelf information (Salvatteci et al., 2014a). These upper mud lenses
112 are characterized by fine grain size, a diatomaceous, hemiplegic mud with high organic carbon,
113 and the absence of erosive and bioturbation processes.

114 The Pisco continental shelf sediments are a composite of laminated structures characterized by
115 an array of more or less dense sections of dark and light millimetric laminae (Brodie and Kemp,
116 1994; Salvatteci et al., 2014a; Sifeddine et al., 2008). The laminae structure and composition
117 result from a complex interplay of factors including the terrigenous material input (both aeolian
118 and fluvial), the upwelling productivity, and associated particle export to the seafloor (Brodie
119 and Kemp, 1994; Salvatteci et al., 2014a). The anoxic conditions favored by an intense OMZ
120 (Gutiérrez et al., 2006) and weak current activity at some areas (Reinhardt et al., 2002; Suess et
121 al., 1987) favor the preservation of paleo-environmental signals and consequently a successful
122 recording of the environmental and climate variability.

123 Along the Peruvian coast, lithogenic fluvial material is supplied by a series of large rivers that
124 are more significant to the north of the study area (Lavado Casimiro et al., 2012; McPhillips et
125 al., 2013; Morera et al., 2011; Rein, 2005; Scheidegger and Krissek, 1982; Unkel et al., 2007).
126 In fact, Smith, (1983) concluded that sedimentary material can be transported for long distances
127 in an opposite direction of prevailing winds and surface currents in upwelling zones. In fact, the
128 coastal circulation off Peru is dominated by the poleward Peru-Chile undercurrent (PCUC),
129 which flows over the outer continental shelf and upper continental slope, whereas the
130 equatorward Peru coastal current is limited to a few dozens of meters in the surface layer
131 (Chaigneau et al., 2013). On the other hand, several works have shown that precipitation, fluvial
132 input discharge (Bekaddour et al., 2014; Bendix et al., 2002; Lavado-Casimiro and Espinoza,
133 2014), and the PCUC increase during the El Niño events (Hill et al., 1998; Strub et al., 1998;
134 Suess et al., 1987). These observations suggest a potential for the fluvial particles to spread over
135 the continental margin under wet paleoclimatic conditions (e.g., El Niño or El Niño-like).
136 Lithogenic material in the study area might also originate from wind-driven dust storms or
137 “Vientos Paracas”, which are more frequent and intense during Austral winters (Escobar
138 Baccaro, 1993; Gay, 2005; Haney and Grolier, 1991) and by the saltation and suspension
139 mechanisms with which this material reaches the continental shelf.

140 **3. Materials and Methods**

141 **3.1. Stacked record.**

142 The B040506 “B06” (14° 07.90’ S, 76° 30.10’ W, 299 m water depth) and the G10-GC-01
143 “G10” (14° 22.96’ S, 076° 23.89’ W, 313 m water depth) sediment cores were retrieved from
144 the central Peruvian continental shelf in 2004 during the Paleo2 cruise onboard the Peruvian
145 José Olaya Balandra vessel (IMARPE) and in 2007 during the Galathea-3 cruise, respectively
146 (Fig. 1A). We compared the age models and performed a laminae cross-correlation between the
147 two cores in order to develop a continuous record for the last millennium (Salvatteci et al.,
148 2014a) (Fig. 1S). The choice of these two cores was based on previous detailed stratigraphic
149 investigations and available complementary multi-proxy reconstructions (Gutiérrez et al., 2006,
150 2009; Salvatteci et al., 2012, 2014a, 2014b; Sifeddine et al., 2008). The boxcore B06 (0.75 m
151 length) is a laminated core with a visible slump at ~52cm and 3 thick homogeneous deposits
152 (1.5 to 5.0 cm thick) identified in the SCOPIX images. These intervals were not considered in
153 our study (Fig. 1S). The presence of filaments of the giant sulphur bacteria *Thioploca* spp in the
154 top of core B06 confirms the successful recovery of the sediment water interface.

155 According to the biogeochemical analysis in Gutierrez et al., (2009) (i.e., Palynofacies, Oxygen
156 Index (Rock-Eval), total organic carbon and $\delta^{13}\text{C}$), B06 is characterized by a distinctive shift at
157 ~30 cm, more details are provided by Sifeddine, et al. (2008) and Salvatteci et al., (2014a). The
158 age model of B06 was inferred from five ^{14}C -calibrated AMS age distributions (Fig. 1S),
159 showing that this core covers the last ~700 yr. For the last century, which is recorded only by
160 B06, the age model was based on downcore natural excess ^{210}Pb and ^{137}Cs distributions and
161 supported by bomb-derived ^{241}Am distributions (Fig. 2S and Gutiérrez et al., (2009). The mass
162 accumulation rate after ca. 1950AD was $0.036\pm 0.001 \text{ gcm}^{-2} \text{ y}^{-1}$ and before ca. 1820AD was
163 $0.022\pm 0.001 \text{ gcm}^{-2} \text{ y}^{-1}$. On the other hand, the G10 is a gravity laminated sediment core of 5.22
164 m presenting six units and exhibiting some minor slumping. The G10 age model was based on
165 thirty one samples of ^{14}C -calibrated AMS age distributions, showing that the core covers the
166 Holocene period (Salvatteci et al., 2014b, 2016). Here we used only a laminated section
167 between ~18 - 45 cm that chronologically covered part of the MCA period (from ~1050 to
168 1500) and presented no slumps (Fig. 1S).

169 The spatial regularity of the initial core sampling combined with the naturally variable
170 sedimentation rate implied variable time rates between samples (150 samples in total). Each
171 sample is 0.5 cm thick in B06 and usually includes 1-2 laminae. On the other hand in core G10
172 each sample is 1 cm thick including 3-4 laminae. The results considering the sedimentation rates
173 showed that the intervals during MCA, LIA and CWP span between 18, 7, and 3 years,
174 respectively. Because of differences in the subsampling thickness between cores and variable
175 sedimentation rates, results are binned by 20 year intervals (the lowest time resolution among
176 samples) after linear interpolation and 20-yr running mean of the original data set.

177 **3.2. Grain size analyses**

178 To isolate the mineral terrigenous fraction, organic matter, calcium carbonate and biogenic
179 silica were successively removed from approximately 100 mg of bulk sediment sample using
180 H₂O₂ (30% at 50°C for 3 to 4 days), HCl (10% for 12 hours) and Na₂CO₃ (1 M at 90°C for 3
181 hours) respectively. Between each chemical treatment, samples were repeatedly rinsed with
182 deionized water and centrifuged at 4000 rpm until neutral pH. After pre-treatment, the grain size
183 distribution was determined with an automated image analysis system (model FPIA3000,
184 Malvern Instruments). This system is based on a CCD (Charge Coupled Device) camera that
185 captures images of all of the particles homogeneously suspended in a dispersal solution by
186 rotation (600 rpm) in a measurement cell. After magnification ($\times 10$), particle images are
187 digitally processed and the equivalent spherical diameter (defined as the diameter of the
188 spherical particle having the same surface as the measured particle) is determined. The optical
189 magnification used ($\times 10$) allows the counting of particles with equivalent diameters between 0.5
190 and 200 μm . Prior to the FPIA analysis, all samples were sieved with a 200- μm mesh in order to
191 recover coarser particles. Since particles $> 200 \mu\text{m}$ were never found in any samples, the grain
192 size distribution obtained by the FPIA method reliably represents the full particle size range in
193 the sediment. A statistically significant number of particles (hundreds of thousands up to
194 300,000) are automatically analyzed by FPIA, providing particle size information comparable to
195 that obtained with a laser granulometer along with images of the individual particles. Using the
196 images to check the efficiency of the pre-treatments, we ensured that both organic matter and
197 biogenic silica had been completely removed from all the samples. Finally, particle countings
198 were binned into 45 different size bins between 0.5 and 200 micron instead of the 225 set by the
199 FPIA manufacturer in order to reduce errors related to the presence of very few particles in
200 some of the preselected narrow bins. Grain size distributions are expressed as (%) volume
201 distributions.

202 **3.3. Determining sedimentary components and the de-convolution fitting model**

203 As different particle transport/deposition processes are known to influence the grain-size
204 distribution of the lithic fraction of sediment (e.g. Holz et al., 2007; Pichevin et al., 2005; Prins
205 et al., 2007; Stuut et al., 2005, 2002; Sun et al., 2002; Weltje and Prins, 2003, 2007; Weltje,
206 1997), identifying the individual components of the polymodal grain size distribution is decisive
207 for paleoenvironmental reconstructions. The numerical characteristics [i.e., amplitude A,
208 geometric mean diameter (Gmd), and geometric standard deviation (Gsd) of the individual grain
209 size populations whose combination forms the overall grain size distribution] were determined
210 for all samples using the iterative least-square method of Gomes et al. (1990). This fitting
211 method aims to minimize the squared difference between the measured volume-grain size

212 distribution and the one computed from a mathematical expression based on log-normal
213 function. The number of individual grain size populations to be used is determined by the
214 operator, and all statistical parameters (A, Gmd and Gsd) are allowed to change from one
215 sample to another. This process presents a strong advantage compared to end-member modeling
216 (e.g., Weltje 1997) in which the individual grain size distributions are maintained constant over
217 the whole time series, the only fitting parameter being the relative amplitude, A. Indeed, it is
218 unlikely that the parameters that govern both transport and deposition of lithogenic material,
219 and therefore grain size of particles, remain constant over time. In turn, variations of these
220 parameters are expected to induce change of the grain size distribution parameters such as Gmd
221 and Gsd.

222 **4. Results and discussion**

223 **4.1. Basis for interpretation**

224 Both sediment cores (B06 and G10) exhibit roughly bimodal grain-size distribution presenting
225 significant variation in amplitude and width. These modes correspond to fine-grain-size classes
226 from ~3 to 15 μm and coarser grain size classes between ~50 and 120 μm (Fig. 3S). A principal
227 component analysis (PCA) based on the Wentworth (1922) grain-size classification identifies
228 four modes that could explain the total variance of the dataset (Fig. 4S). The measured and
229 computed grain size distributions show high correlations ranging from $R^2=0.75$ to 0.90, attesting
230 that using 4 grain size modes is well adapted to our sediment samples and that the computed
231 ones may be reliable for further interpretation (Fig. 2). Lower correlations only occurred for 6
232 samples that are characterized by small proportions of terrigenous material compared to
233 biogenic silica, organic matter and carbonates. In these cases, the number of lithic particles
234 remaining after chemical treatments was small, which increased the associated relative error.
235 However, these samples have been included in the data set since they all presented a high
236 contribution of coarser particles.

237 Grain size parameters are presented in Table 1. The first mode (M1), with a Gmd of
238 approximately $3 \pm 1 \mu\text{m}$, and the second one (M2), with a Gmd of $10 \pm 2 \mu\text{m}$, are characterized
239 by large Gsd ($\sim 2\sigma$), indicating a low degree of sorting. Such low degree of sorting suggests a
240 slow and continuous depositional process as occurs in other environments (Sun et al., 2002).
241 The coarsest modes M3 and M4 display mean Gmd values of $54 \pm 12 \mu\text{m}$ and $91 \pm 13 \mu\text{m}$,
242 respectively. These modes present Gsd values close to 1σ . The Gmd values of the two coarsest
243 modes are consistent with the optimal grain size transported under conditions favorable to soil
244 erosion (lack of vegetation, low threshold friction velocity, surface roughness and low soil
245 moisture) and low wind friction velocity (Iversen and White, 1982; Kok et al., 2012;
246 Marticorena and Bergametti, 1995; Marticorena, 2014; Shao and Lu, 2000). Such conditions

247 prevail in the studied area because the central coastal Peru consists of a sand desert area
248 characterized by the absence of rain, a lack of vegetation and persistent wind (Gay, 2005; Haney
249 and Grolier, 1991).

250 In the vicinity of desert areas, where wind-blown transport prevails, particles with grain size as
251 high as $\sim 100 \mu\text{m}$ can accumulate in marine sediments (e.g., Flores-Aqueveque et al., 2015;
252 Stuut et al., 2007) or even in lacustrine sediments (An et al., 2012). Indeed, Stuut et al., (2007)
253 reported the presence of distributions typical of wind-blown particles with $\sim 80 \mu\text{m}$ grain size
254 ($\sim 29^\circ\text{S}$ North Chile) that is consistent with our results. In the studied area, the emission and the
255 transport of mineral particles are related to the strong wind events called “Paracas”. Paracas dust
256 emission is a local seasonal phenomenon that preferentially occurs in winter (July-September)
257 and is due to an intensification of the local surface winds (Escobar Baccaro, 1993; Haney and
258 Grolier, 1991; Schweigger, 1984). The pressure gradient of sea level between $15^\circ\text{--}20^\circ\text{S}$, 75°W
259 is the controlling factor of Paracas winds (Quijano, 2013), along with local topography (Gay,
260 2005). Coarse particles found in continental sediments off Pisco cannot have a fluvial origin
261 because substantial hydrodynamic energy is necessary to mobilize particles of this size ($50\text{--}100$
262 μm), and this region is devoid of large rivers (Reinhardt et al., 2002; Scheidegger and Kriesek,
263 1982; Suess et al., 1987).

264 Therefore, the coarsest modes (M3 and M4) can be interpreted as markers of aeolian transport
265 resulting from surface winds and emission processes (Flores-Aqueveque et al., 2015; Hesse and
266 McTainsh, 1999; Marticorena and Bergametti, 1995; McTainsh et al., 1997; Sun et al., 2002)
267 and indicate a local and proximal aeolian source (i.e., Paracas winds). This interpretation is in
268 contrast to the Atacama Desert source suggested by Ehlert et al., (2015) and Molina-Cruz,
269 (1977). Ehlert et al. (2015), who used the same sediment core (B06), and also indicated
270 difficulties in the interpretation of the detrital Sr isotopic signatures as an indicator of the
271 terrigenous sources. These difficulties can be associated with the variability of the $^{87}\text{Sr}/^{86}\text{Sr}$ due
272 to grain size (Meyer et al., 2011). The finest M1 component ($\sim 3 \mu\text{m}$) may be linked to both
273 aeolian and fluvial transport mechanisms. Thus, because its origin is difficult to determine, and
274 because its trend appears as relatively independent from the other components, we do not
275 further use it.

276 The M2 component ($\sim 10 \mu\text{m}$) is interpreted as an indicator of fluvial transport (Koopmann,
277 1981; McCave et al., 1995; Stuut and Lamy, 2004; Stuut et al., 2002, 2007). Indeed, this is
278 consistent with the report by Stuut et al., (2007) for the fluvial mud ($\sim 8 \mu\text{m}$) in the South of
279 Chile ($>37^\circ\text{S}$) where the terrigenous input is dominated by fluvial origins. A fluvial origin of
280 this M2 component is also supported by showing the same trend in the geochemical proxies,
281 such as radiogenic isotope compositions of detrital components (Ehlert et al., 2015), mineral

282 fluxes (Sifeddine et al., 2008) or %Ti (Salvatteci et al., 2014b), indicating more terrigenous
283 transport during the LIA, when humid conditions were dominant. The M2 component is
284 interpreted as being linked to river material discharge, mostly from the north Peruvian coast,
285 and redistribution by the PCUC and bottom currents (Montes et al., 2010; Rein et al., 2004;
286 Scheidegger and Krissek, 1982; Unkel et al., 2007).

287 **4.2. Aeolian and fluvial input variability during the past ~1000 yr**

288 Grain size component (M2, M3 and M4; Table 1) variations in the composite records (B06 and
289 G10) express changes in wind stress and fluvial runoff at multi-decadal to centennial scales
290 during the last millennium. The sediments deposited during the MCA exhibit two contrasting
291 patterns of grain size distributions. A first sequence dated from 1050 to 1170 AD has, low
292 values of D_{50} (i.e., median grain size) that vary around $16 \pm 6 \mu\text{m}$ and are explained by $50 \pm$
293 14% M2, $16 \pm 8\%$ M3, $21 \pm 5\%$ M4 and $13 \pm 5\%$ M1 contributions. A second sequence, dated from
294 1170 to 1450 AD, was marked by high values of D_{50} in the range of $34 \pm 18 \mu\text{m}$, with average
295 contributions of $36 \pm 8\%$ for M2, $21 \pm 10\%$ for M3, $29 \pm 15\%$ for M4 and $14 \pm 6\%$ for M1.
296 These results indicate high variability of transport of particles during the MCA, with more
297 fluvial sediment discharge from 1050 to 1170, followed by an aeolian transport increase between
298 1170 and 1450 AD (Fig. 3).

299 During the LIA (1450 – 1800 AD), the deposited particles were dominated by fine grain sizes
300 with a D_{50} varying around an average of $15 \mu\text{m}$, explained by $53 \pm 15\%$ M2 contribution. In
301 contrast, the contribution of M3 averaged $19 \pm 9\%$ and ranged from 4 to 45%, whereas M4
302 showed an average contribution of $14 \pm 11\%$ and varied from 0 to 44% during the same period.
303 The dominant contribution of the finest-sized particles of M2 suggests a high fluvial terrigenous
304 input to the Peruvian continental shelf. It is important to note that M2 contributions increased
305 from the beginning to the end of the LIA at ~1800 AD, suggesting a gradual increase in fluvial
306 sediment discharge input related to the enhancement of the continental precipitation (Fig. 3C).
307 Indeed, during the LIA, our results confirm previous interpretations of wet conditions along the
308 Peruvian coast (Gutiérrez et al., 2009; Salvatteci et al., 2014b; Sifeddine et al., 2008). These
309 results also imply that this period was characterized by weak surface winds and hence a weaker
310 coastal upwelling.

311 Subsequently, D_{50} variations show multidecadal variability during the last ~200 yr that is
312 divided into three distinctive periods. The first one from ~1800 to 1850 AD shows dominance
313 of coarse particles around $50 \mu\text{m}$, explained by the high contribution of M3 and M4 (up to 45%
314 and 50% respectively) during this period. These results suggest a period of drier climate and
315 very strong wind conditions. The second one from 1850 to 1900 AD displays values around ~20
316 μm explained by ~40% of M2, ~20% of M3 and ~20% of M4 that suggests that fluvial sediment

317 discharge was the dominant transport mechanism, although not as significant as during the LIA.
318 The third period spans from 1900 AD to the final part of record and covers the CWP. Our
319 results reveal a dominance of coarse particles during the most of this period (D50 up to of 80
320 μm) that arise from high contributions of M3 and M4 (~40% and ~50% respectively). However
321 a clear decrease of the D50 is displayed at the end of this period that is explained by a decrease
322 of contributions of the aeolian component M4 (~20%), although the contribution of M3 and M2
323 remain relatively stable (~25% and 30%, respectively). These conditions display no clear
324 dominance of a given transport mode during this time. In addition, markedly coarser particles in
325 the M4 component were very common during this time (the last 200yr), indicating a strong
326 probability of extreme wind stress events (Fig. 3F).

327 **4.3. Climatic interpretations**

328 Our findings suggest a combination of regional and local atmospheric circulation mechanism
329 changes that controlled the pattern of sedimentation in the study region. Our record is located
330 under the contemporary seasonal Paracas dust storm path, but it also records discharged fluvial
331 muds that are supplied by the rivers along the Peruvian coast. Hence, this record is particularly
332 well suited for a reconstruction of continental runoff/wind intensity in the central Peruvian
333 continental shelf during the last millennium. The interpretation of the changes in the single
334 records of the components (M2, M3 and M4) and their associations (e.g., ratios) can reflect
335 paleoclimatic variations in response to changes in atmospheric conditions. Here, we used the
336 ratio between the aeolian components, defined as the contribution of the stronger winds over
337 total wind variability: $M4/(M3+M4)$. We consider this ratio as a proxy of the local wind surface
338 intensity and thus as of the SPSH atmospheric circulation (Fig. 4A). Previous studies have
339 similarly and successfully used grain-size fraction ratios as paleoclimate proxies of atmospheric
340 conditions and circulation to explain other sediment records (Holz et al., 2007; Huang et al.,
341 2011; Prins, 1999; Shao et al., 2011; Stuut et al., 2002; Sun et al., 2002; Weltje and Prins,
342 2003).

343 As explained above, the MCA was characterized by a sine-like peak structure that depicts two
344 different climate stages. During the first stage spanning from ~1050 to 1170 AD the fluvial
345 input show a peak centered at 1120 AD linked to a precipitation increase accompanied by a
346 decrease in wind intensity. Those results suggest a southward ITCZ displacement (Fig. 4E) as a
347 response to more El Niño like conditions as suggested by Rustic et al., (2015) (Fig 4 G and H).
348 In contrast, during the second stage the surface winds had their greatest intensity with a peak
349 centered at ~1200 AD as a consequence of displacement of the ITCZ-SPSH system. The
350 displacement of the SPSH core towards the eastern South American coast intensified alongshore
351 winds as a regional response to stronger Walker circulation. These features are in agreement

352 with the ocean thermostat mechanism proposed by Clement et al., (1996). This mechanism
353 produces a shallow thermocline in the eastern Pacific (Fig. 4G and H) and consequently more
354 intense upwelling conditions and a stronger OMZ offshore of Pisco recorded in low values of
355 the Re/Mo ratio (Fig. 4D). These two patterns (i.e., enhanced fluvial transport/enhanced wind
356 intensity) might have been triggered by the expression of Pacific variability at multidecadal
357 timescales with the combined action of the Atlantic Multidecadal Oscillation (AMO). Indeed
358 other works provide evidence during the MCA for low South American Monsoon System
359 (SAMS) activity at multidecadal timescales driven by the AMO (Fig. 4F) (Apaéstegui et al.,
360 2014; Bird et al., 2011; Reuter et al., 2009). Thus, besides the displacement of the ITCZ', the
361 AMO could have modulated Walker circulation at a multidecadal variability during the MCA
362 through mechanisms such as those described by McGregor et al., (2014) and Timmermann et al.,
363 (2007).

364 Our results, combined with other paleo-reconstructions, suggest that the LIA was accompanied
365 by a weakening of the regional atmospheric circulation and of the upwelling favorable winds.
366 During the LIA, the mean climate state was controlled by a gradual intensification of the fluvial
367 input of sediments to the continental shelf, thus indicating more El Niño-like conditions (Fig.
368 4B). These features are confirmed by an increase of the terrigenous sediment flux, as described
369 by Sifeddine et al. (2008) (Fig 4C) and Gutierrez et al., (2009) and by changes of the radiogenic
370 isotopic composition of the terrigenous fraction (Ehlert et al., 2015). These wet conditions are
371 also marked by an intensification of the South American Monsoon System (SAMS) and the
372 southern meridional displacement of the ITCZ, as evidence by paleo-precipitation records in the
373 Andes and in the Cariaco Trench (Apaéstegui et al., 2014; Haug et al., 2001; Peterson and
374 Haug, 2006) (Fig. 4E). At the same time, a prevalence of weak surface winds (Fig.4A) and an
375 increase of subsurface oxygenation driving sub-oxic conditions in the surface sediment are
376 recorded (Fig. 4D). These characteristics also support the hypothesis of the ITCZ-SPSH
377 southern meridional displacement and are consistent with a weakening of the Walker circulation
378 (Fig. 4G).

379 The transition period between the LIA and CWP appears as an abrupt event showing a
380 progressive positive anomaly in the wind intensity synchronous with a rapid decrease in fluvial
381 input to the continental shelf (Fig. 4A and B). This transition suggests a rapid change of
382 meridional (ITCZ-SPSH) and zonal (Walker) circulation interconnection, which controls the
383 input of terrigenous material (Fluvial/Aeolian). Gutiérrez et al. (2009) found evidence of a large
384 reorganization in the tropical Pacific climate with immediate effects on ocean biogeochemical
385 cycling and ecosystem structure at the transition between the LIA and CWP. The increase in the
386 regional wind circulation that favors aeolian erosive processes simultaneously leads to an
387 increase in the OMZ intensity related to upwelling intensification.

388 Finally, during the CWP (~1900 A.D. to present), a trend to steadying of low fluvial input (Fig.
389 4B) was combined with an increase in wind intensity (Fig. 4A) that was coupled to a strong
390 OMZ. This setting suggests the northernmost ITCZ-SPSH system position. This hypothesis is
391 supported by other studies on the continental shelf of Peru (Salvatteci et al., 2014b) and also in
392 the Eastern Andes where a decrease in rainfall of between ~10 – 20% relative to the LIA was
393 reported for the last century (Reuter et al., 2009). Enhancement of wind intensity is also
394 consistent with the multidecadal coastal cooling and increase of upwelling productivity since
395 the late nineteenth century (Gutiérrez et al., 2011; Salvatteci et al., 2014b; Sifeddine et al.,
396 2008) and confirms the relations between the intensification of the upwelling activity induced
397 by the variability of the regional wind intensity from SPSH displacement.

398 The increase in the wind intensity over the past two centuries likely represents a result of the
399 modern positioning of the ITCZ – SPSH system and the associated intensification of the local
400 and regional winds (Fig. 4A). The contributions of aeolian deposition material (Fig. 3E and F)
401 and in consequence the wind intensity and its variability during the last 100 yr are stronger than
402 during the second sequence of the MCA (Fig. 4A) under similar conditions (i.e., position of the
403 ITCZ-SPSH system). This variability implies a forcing mechanism in addition to the
404 enhancement of the wind intensity, one that may be related to the current climate change
405 conditions (Bakun, 1990; England et al., 2014; Sydeman et al., 2014). Moreover, during the
406 CWP, the wind intensity showed a direct-relation with OMZ strength (Fig. 4A and D) that
407 suggests an increase in the zonal gradient and thus in the Walker circulation on a multidecadal
408 scale.

409 Our record shows that on a centennial scale, the fluvial input changes are driven by the
410 meridional ITCZ position and a weak gradient of the Walker circulation, consistent with El
411 Niño like conditions. In contrast, variations of the surface wind intensity are linked to the
412 position of the SPSH modulated by both the meridional variation of the ITCZ and the
413 intensification of the zonal gradient temperature related with the Walker circulation and
414 expressing La Niña like conditions. A clear relation between the zonal circulation and wind
415 intensity at a centennial time scale is displayed. All these features modulate the biogeochemical
416 behavior of the Peruvian upwelling system.

417 **Conclusions**

418 Study of the grain size distribution in laminated sediments from the Pisco Peruvian shelf has
419 allowed the reconstruction of changes in wind intensity and terrigenous fluvial input at
420 centennial and multidecadal time scales during the last millennium. The long-term variation of
421 M2 (~10 μ m) mode is an indicator of hemipelagic fluvial input related to the regional
422 precipitation variability. Meanwhile, the M3 (54 \pm 11 μ m) and M4 (91 \pm 11 μ m) components are

423 related to aeolian transport and thus with both local and regional wind intensity. The temporal
424 variations of these fractions indicate that the MCA and CWP periods were characterized by an
425 increment in the coarse particle transport (M3 and M4) and thus an enhancement of the surface
426 wind intensity, whereas the LIA was characterized by stronger fluvial input as evidence from an
427 increase of fine (M2) particles. Comparison between records reveals a coherent match between
428 the meridional displacement of the ITCZ-SPSH system and the regional fluvial and aeolian
429 terrigenous input variability. The ITCZ-SPSH system northern displacement during the second
430 period of the MCA and the CWP was associated with the intensification of the Walker cell and
431 La Niña Like conditions, resulting in stronger winds, upwelling-favorable conditions, enhanced
432 marine productivity and greater oxygen depletion in the water column. In contrast, the
433 southward migrations of the ITCZ-SPSH system during the LIA correspond to an enhancement
434 to the South American Monsoon circulation and El Niño like conditions, driving the increase in
435 the precipitation and the terrigenous fluvial input to the Pisco continental shelf, lower
436 productivity and increased oxygenation. Two patterns observed during the MCA, respectively
437 marked by fluvial intensification and wind intensification, could have been forced by Pacific
438 Ocean variability at multidecadal timescales. Further studies of the paleo-wind reconstruction at
439 high time-resolution, combined with model simulation, are needed to better understand the
440 interplay between the Pacific and Atlantic Ocean connection on climate variability as evidenced
441 by Mcgregor et al., (2014) in the modern Pacific climate pattern.

442 **5. Acknowledgements**

443 This work was supported by the International Joint Laboratory "PALEOTRACES" (IRD-
444 France, UPMC-France, UFF-Brazil, UA-Chile, UPCH-Peru), the Department of Geochemistry
445 of the Universidade Federal Fluminense-UFF (Brazil), the ALYSES analytical platform
446 (IRD/UPMC, supported by grants from Région Ile-de-France), the Peruvian Marine Research
447 Institute (IMARPE) and the Geophysical Peruvian Institute (IGP). It was also supported by the
448 collaborative project Chaire Croisée PROSUR (IRD). We deeply thank the CAPES-Brazil for
449 the scholarship to Francisco Briceño Zuluaga. We give special thanks to Dr. Ioanna Bouloubassi
450 and Dr. Phil Meyers by their comments and suggestions. We are also grateful to the
451 anonymous reviewers for their constructive and helpful suggestions to improve this manuscript.

452 **3 7. Bibliography**

453 An, F., Ma, H., Wei, H. and Lai, Z.: Distinguishing aeolian signature from lacustrine sediments
454 of the Qaidam Basin in northeastern Qinghai-Tibetan Plateau and its palaeoclimatic
455 implications, *Aeolian Res.*, 4, 17–30, doi:10.1016/j.aeolia.2011.12.004, 2012.

456 Apaéstegui, J., Cruz, F. W., Sifeddine, A., Vuille, M., Espinoza, J. C., Guyot, J. L., Khodri, M.,
457 Strikis, N. and Perú, G.: Hydroclimate variability of the northwestern Amazon Basin near the
458 Andean foothills of Peru related to the South American Monsoon System during the last 1600

- 459 years, *Clim. Past*, 10(1), 1967–1981, doi:10.5194/cp-10-1967-2014, 2014.
- 460 Bakun, a: Global climate change and intensification of coastal ocean upwelling., *Science*,
461 247(4939), 198–201, doi:10.1126/science.247.4939.198, 1990.
- 462 Bekaddour, T., Schlunegger, F., Vogel, H., Delunel, R., Norton, K. P., Akçar, N. and Kubik, P.:
463 Paleo erosion rates and climate shifts recorded by Quaternary cut-and-fill sequences in the Pisco
464 valley, central Peru, *Earth Planet. Sci. Lett.*, 390, 103–115, doi:10.1016/j.epsl.2013.12.048,
465 2014.
- 466 Bendix, A., Bendix, J., Gämmerler, S., Reudenbach, C. and Weise, S.: The El Niño 1997 / 98 as
467 seen from space - rainfall retrieval and investigation of rainfall dynamics with Goes-8 and
468 TRMM Data, in *The 2002 EUMETSAT Meteor. Satellite Conf.*, Dublin, Ireland 02-06 Sept.
469 2002, EUM P 36, pp. 647–652., 2002.
- 470 Bird, B. W., Abbott, M. B., Vuille, M., Rodbell, D. T., Stansell, N. D. and Rosenmeier, M. F.: A
471 2,300-year-long annually resolved record of the South American summer monsoon from the
472 Peruvian Andes., *Proc. Natl. Acad. Sci. U. S. A.*, 108(21), 8583–8,
473 doi:10.1073/pnas.1003719108, 2011.
- 474 Bloemsmä, M. R., Zabel, M., Stuu, J. B. W., Tjallingii, R., Collins, J. a. and Weltje, G. J.:
475 Modelling the joint variability of grain size and chemical composition in sediments, *Sediment.*
476 *Geol.*, 280, 135–148, doi:10.1016/j.sedgeo.2012.04.009, 2012.
- 477 Böning, P. and Brumsack, H.: Geochemistry of Peruvian near-surface sediments, *Geochim.*
478 *Cosmochim. Acta*, 68(21), 4429–4451, doi:10.1016/j.gca.2004.04.027, 2004.
- 479 Brodie, I. and Kemp, A. E. S.: Variation in Biogenic and Detrital Fluxes and Formation of
480 Laminae in Late Quaternary Sediments from the Peruvian Coastal Upwelling Zone, *Mar. Geol.*,
481 116(3-4), 385–398, doi:10.1016/0025-3227(94)90053-1, 1994.
- 482 Chaigneau, A., Dominguez, N., Eldin, G., Vasquez, L., Flores, R., Grados, C. and Echevin, V.:
483 Near-coastal circulation in the Northern Humboldt Current System from shipboard ADCP data,
484 *J. Geophys. Res. Ocean.*, 118(10), 5251–5266, doi:10.1002/jgrc.20328, 2013.
- 485 Clement, A. C., Seager, R., Cane, M. a. and Zebiak, S. E.: An ocean dynamical thermostat, *J.*
486 *Clim.*, 9(9), 2190–2196, doi:10.1175/1520-0442(1996)009<2190:AODT>2.0.CO;2, 1996.
- 487 Ehlert, C., Grasse, P., Gutiérrez, D., Salvatucci, R. and Frank, M.: Nutrient utilisation and
488 weathering inputs in the Peruvian upwelling region since the Little Ice Age, *Clim. Past*, 11,
489 187–202, doi:10.5194/cpd-10-3357-2014, 2015.
- 490 England, M. H., McGregor, S., Spence, P., Meehl, G. a., Timmermann, A., Cai, W., Gupta, A.
491 Sen, McPhaden, M. J., Purich, A. and Santoso, A.: Recent intensification of wind-driven
492 circulation in the Pacific and the ongoing warming hiatus, *Nat. Clim. Chang.*, 4(3), 222–227,
493 doi:10.1038/nclimate2106, 2014.
- 494 Escobar Baccaro, D. F.: Evaluacion climatologica y sinoptica del fenómeno de vientos Paracas,
495 Universidad Nacional Agraria La Molina, Lima-Peru., 1993.
- 496 Flores-Aqueveque, V., Alfaro, S. C., Caquineau, S., Foret, G., Vargas, G. and Rutllant, J. a.:
497 Inter-annual variability of southerly winds in a coastal area of the Atacama Desert: implications
498 for the export of aeolian sediments to the adjacent marine environment, *Sedimentology*, 59(3),
499 990–1000, doi:10.1111/j.1365-3091.2011.01288.x, 2012.
- 500 Flores-Aqueveque, V., Alfaro, S., Vargas, G., Rutllant, J. a. and Caquineau, S.: Aeolian
501 particles in marine cores as a tool for quantitative high-resolution reconstruction of upwelling
502 favorable winds along coastal Atacama Desert, Northern Chile, *Prog. Oceanogr.*, 134, 244–255,
503 doi:10.1016/j.pcean.2015.02.003, 2015.
- 504 Garreaud, R. D. and Falvey, M.: The coastal winds off western subtropical South America in
505 future climate scenarios, *Int. J. Climatol.*, 29(4), 543–554, doi:10.1002/joc.1716, 2009.

- 506 Gay, S. P.: Blowing sand and surface winds in the Pisco to Chala Area, Southern Peru, *J. Arid Environ.*, 61(1), 101–117, doi:10.1016/j.jaridenv.2004.07.012, 2005.
- 508 Gomes, L., Bergametti, G., Dulac, F. and Ezat, U.: Assessing the actual size distribution of
509 atmospheric aerosols collected with a cascade impactor, *J. Aerosol Sci.*, 21(1), 47–59,
510 doi:10.1016/0021-8502(90)90022-P, 1990.
- 511 Gutiérrez, D., Bouloubassi, I., Sifeddine, A., Purca, S., Goubanova, K., Graco, M., Field, D.,
512 Méjanelle, L., Velazco, F., Lorre, A., Salvateci, R., Quispe, D., Vargas, G., Dewitte, B. and
513 Ortlieb, L.: Coastal cooling and increased productivity in the main upwelling zone off Peru
514 since the mid-twentieth century, *Geophys. Res. Lett.*, 38(7), 1–6, doi:10.1029/2010GL046324,
515 2011.
- 516 Gutiérrez, D., Sifeddine, A., Field, D., Ortlieb, L., Vargas, G., Chaves, F., Velazco, F., Ferreira,
517 V., Tapia, P., Salvateci, R., Boucher, H., Morales, M. C., Valdes, J., Reyss, J., Campusano, A.,
518 Boussafir, M., Mandeng-Yogo, M., Garcia, M. and Baumgartner, T.: Rapid reorganization in
519 ocean biogeochemistry off Peru towards the end of the Little Ice Age, *Biogeosciences*, 6, 835–
520 848, 2009.
- 521 Gutiérrez, D., Sifeddine, A., Reyss, J., Vargas, G., Velasco, F., Salvateci, R., Ferreira, V.,
522 Ortlieb, L., Field, D., Baumgartner, T., Boussafir, M., Boucher, H., Valdes, J., Marinovic, L.,
523 Soler, P. and Tapia, P.: Anoxic sediments off Central Peru record interannual to multidecadal
524 changes of climate and upwelling ecosystem during the last two centuries., *Adv. Geosci.*, 6,
525 119–125, 2006.
- 526 Haney, E. M. and Grolier, M. J.: Geologic map of major Quaternary eolian features, northern
527 and central coastal Peru, *United States Geol. Surv. Misc. Investig.*, I-2162, 1991.
- 528 Haug, G. H., Hughen, K. a, Sigman, D. M., Peterson, L. C. and Röhl, U.: Southward migration
529 of the intertropical convergence zone through the Holocene., *Science*, 293(5533), 1304–8,
530 doi:10.1126/science.1059725, 2001.
- 531 Hesse, P. P. and McTainsh, G. H.: Last Glacial Maximum to Early Holocene Wind Strength in
532 the Mid-latitudes of the Southern Hemisphere from Aeolian Dust in the Tasman Sea, *Quat.*
533 *Res.*, 52(3), 343–349, doi:10.1006/qres.1999.2084, 1999.
- 534 Hill, E. A., Hickey, B. M., Shillington, F. A., Strub, P. T., Brink, K. H., Barton, E. D. and
535 Thomas, A. C.: Eastern Ocean Boundaries coastal segment (E), in *The Sea*, Vol 11, vol. II,
536 edited by A. Robinson and K. Brink, pp. 29–67, John Wiley & Sons Ltd., 1998.
- 537 Holz, C., Stuu, J. B. W., Henrich, R. and Meggers, H.: Variability in terrigenous sedimentation
538 processes off northwest Africa and its relation to climate changes: Inferences from grain-size
539 distributions of a Holocene marine sediment record, *Sediment. Geol.*, 202(3), 499–508,
540 doi:10.1016/j.sedgeo.2007.03.015, 2007.
- 541 Huang, X., Oberhänsli, H., von Suchodoletz, H. and Sorrel, P.: Dust deposition in the Aral Sea:
542 implications for changes in atmospheric circulation in central Asia during the past 2000 years,
543 *Quat. Sci. Rev.*, 30(25-26), 3661–3674, doi:10.1016/j.quascirev.2011.09.011, 2011.
- 544 Iversen, J. D. and White, B. R.: Saltation threshold on Earth, Mars and Venus, *Sedimentology*,
545 29, 111–119, doi:10.1111/j.1365-3091.1982.tb01713.x, 1982.
- 546 Kok, J. F., Parteli, E. J. R., Michaels, T. I. and Karam, D. B.: The physics of wind-blown sand
547 and dust, *Reports Prog. Phys.*, 75(10), 106901, doi:10.1088/0034-4885/75/10/106901, 2012.
- 548 Koopmann, B.: Sedimentation von Saharastaub im subtropischen Nordatlantik während der
549 letzten 25.000 Jahre, *Meteor Forsch. ergeb. R. C*, 35, 23–59, 1981.
- 550 Lavado Casimiro, W., Ronchail, J., Labat, D., Espinoza, J. C. and Guyot, J. L.: Basin-scale
551 analysis of rainfall and runoff in Peru (1969–2004): Pacific, Titicaca and Amazonas drainages,
552 *Hydrol. Sci. J.*, 57(4), 625–642, doi:10.1080/02626667.2012.672985, 2012.

- 553 Lavado-Casimiro, W. and Espinoza, J. C.: Impacts of El Nino and La Nina in the precipitation
554 over Peru (1965-2007), *Rev. Bras. Meteorol.*, 29(2), 171–182, doi:10.1590/S0102-
555 77862014000200003, 2014.
- 556 Marticorena, B.: Dust Production Mechanisms, in *Mineral Dust: A Key Player in the Earth*
557 *System*, edited by P. Knippertz and J.-B. Stuut, pp. 93–120, Springer, Dordrecht Heidelberg
558 New York London., 2014.
- 559 Marticorena, B. and Bergametti, G.: Modeling the atmospheric dust cycle: 1. Design of a soil-
560 derived dust emission scheme, *J. Geophys. Res.*, 100(D8), 16415, doi:10.1029/95JD00690,
561 1995.
- 562 McCave, I. N., Manighetti, B. and Robinson, S. G.: Sortable silt and fine sediment
563 size/composition slicing: parameters for palaeocurrent speed and palaeoceanography,
564 *Paleoceanography*, 10(3), 593–610, doi:10.1029/94PA03039, 1995.
- 565 Mcgregor, S., Timmermann, A., Stuecker, M. F., England, M. H. and Merrifield, M.: Recent
566 Walker circulation strengthening and Pacific cooling amplified by Atlantic warming, *Nat. Clim.*
567 *Chang.*, (August), 1–5, doi:10.1038/NCLIMATE2330, 2014.
- 568 McPhillips, D., Bierman, P. R., Crocker, T. and Rood, D. H.: Landscape response to
569 Pleistocene-Holocene precipitation change in the Western Cordillera, Peru: 10 Be
570 concentrations in modern sediments and terrace fills, *J. Geophys. Res. Earth Surf.*, 118(4),
571 2488–2499, doi:10.1002/2013JF002837, 2013.
- 572 McTainsh, G. H., Nickling, W. G. and Lynch, a. W.: Dust deposition and particle size in Mali,
573 West Africa, *Catena*, 29(3-4), 307–322, doi:10.1016/S0341-8162(96)00075-6, 1997.
- 574 Meyer, I., Davies, G. R. and Stuut, J. B. W.: Grain size control on Sr-Nd isotope provenance
575 studies and impact on paleoclimate reconstructions: An example from deep-sea sediments
576 offshore NW Africa, *Geochemistry, Geophys. Geosystems*, 12(3), 14,
577 doi:10.1029/2010GC003355, 2011.
- 578 Molina-Cruz, A.: The relation of the southern trade winds to upwelling processes during the last
579 75,000 years, *Quat. Res.*, 8(3), 324–338, doi:10.1016/0033-5894(77)90075-8, 1977.
- 580 Montes, I., Colas, F., Capet, X. and Schneider, W.: On the pathways of the equatorial
581 subsurface currents in the eastern equatorial Pacific and their contributions to the Peru-Chile
582 Undercurrent, *J. Geophys. Res. Ocean.*, 115(9), 1–16, doi:10.1029/2009JC005710, 2010.
- 583 Morera, S., Condom, T., Crave, A. and Galvez, C.: Tasas de erosión y dinámica de los flujos de
584 sedimentos en la cuenca del río Santa , Perú, *Rev. Peru. Geo-Atmosférica RPGA*, 37(3), 25–37,
585 2011.
- 586 Oppo, D. W., Rosenthal, Y. and Linsley, B. K.: 2,000-year-long temperature and hydrology
587 reconstructions from the Indo-Pacific warm pool., *Nature*, 460(7259), 1113–1116,
588 doi:10.1038/nature08233, 2009.
- 589 Ortlieb, L.: The Documented Historical Record of El Nino Events in Peru: An Update of the
590 Quinn Record (Sixteenth through Nineteenth Centuries), in *El Nino and the Southern*
591 *Oscillation, Multiscale Variability and Global and Regional Impacts*, pp. 207–295., 2000.
- 592 Parkin, D. W. and Shackleton, N. .: Trade wind and temperature correlations down a deep sea
593 core off the Sharan coast, *Nature*, 245, 455–457, 1973.
- 594 Peterson, L. and Haug, G.: Variability in the mean latitude of the Atlantic Intertropical
595 Convergence Zone as recorded by riverine input of sediments to the Cariaco Basin (Venezuela),
596 *Palaeogeogr. Palaeoclimatol. Paleoceanogr.*, 234, 97–113, doi:10.1016/j.palaeo.2005.10.021,
597 2006.
- 598 Pichevin, L., Cremer, M., Giraudeau, J. and Bertrand, P.: A 190 ky record of lithogenic grain-
599 size on the Namibian slope: Forging a tight link between past wind-strength and coastal

600 upwelling dynamics, *Mar. Geol.*, 218(1-4), 81–96, doi:10.1016/j.margeo.2005.04.003, 2005.

601 Prins, M.: Pelagic, hemipelagic and turbidite deposition in the Arabian Sea during the late
602 Quaternary: Unravelling the signals of aeolian and fluvial sediment supply as functions of
603 tectonics, sea-level and climate change by means of end-member modelling of silicic, Utrecht,
604 Universiteit Utrecht., 1999.

605 Prins, M. a., Vriend, M., Nugteren, G., Vandenberghe, J., Lu, H., Zheng, H. and Jan Weltje, G.:
606 Late Quaternary aeolian dust input variability on the Chinese Loess Plateau: inferences from
607 unmixing of loess grain-size records, *Quat. Sci. Rev.*, 26(1-2), 230–242,
608 doi:10.1016/j.quascirev.2006.07.002, 2007.

609 Quijano Vargas, J. J.: Estudio numerico y observacional de la dinámica de Viento Paracas,
610 asociado al transporte eólico hacia el océano frente a la costa de Ica-Perú., Universidad Peruana
611 Cayetano Heredia, Lima - Perú., 2013.

612 Ratmeyer, V., Fischer, G. and Wefer, G.: Lithogenic particle fluxes and grain size distributions
613 in the deep ocean off northwest Africa: Implications for seasonal changes of aeolian dust input
614 and downward transport, *Deep Sea Res. Part I Oceanogr. Res. Pap.*, 46, 1289–1337, 1999.

615 Rein, B.: El Niño variability off Peru during the last 20,000 years, *Paleoceanography*, 20(4),
616 PA4003, doi:10.1029/2004PA001099, 2005.

617 Rein, B.: How do the 1982/83 and 1997/98 El Niños rank in a geological record from Peru?,
618 *Quat. Int.*, 161(1), 56–66, doi:10.1016/j.quaint.2006.10.023, 2007.

619 Rein, B., Lückge, A. and Sirocko, F.: A major Holocene ENSO anomaly during the Medieval
620 period, *Geophys. Res. Lett.*, 31(17), L17211, doi:10.1029/2004GL020161, 2004.

621 Reinhardt, L., Kudrass, H., Lückge, A., Wiedicke, M., Wunderlich, J. and Wendt, G.: High-
622 resolution sediment echosounding off Peru Late Quaternary depositional sequences and
623 sedimentary structures of a current-dominated shelf, *Mar. Geophys. Res.*, 23(1980), 335–351,
624 2002.

625 Reuter, J., Stott, L., Khider, D., Sinha, A., Cheng, H. and Edwards, R. L.: A new perspective on
626 the hydroclimate variability in northern South America during the Little Ice Age, *Geophys. Res.*
627 *Lett.*, 36(21), L21706, doi:10.1029/2009GL041051, 2009.

628 Rustic, G. T., Marchitto, T. M. and Linsley, B. K.: Dynamical excitation of the tropical Pacific
629 Ocean and ENSO variability by Little Ice Age cooling, *Science (80-.)*, 350(6267), 1537–1541,
630 2015.

631 Salvattecì, R., Field, D. B., Baumgartner, T., Ferreira, V. and Gutierrez, D.: Evaluating fish
632 scale preservation in sediment records from the oxygen minimum zone off Peru, *Paleobiology*,
633 38(1), 52–78, doi:10.1666/10045.1, 2012.

634 Salvattecì, R., Field, D., Sifeddine, A., Ortlieb, L., Ferreira, V., Baumgartner, T., Caquineau, S.,
635 Velazco, F., Reyss, J. L., Sanchez-Cabeza, J. A. and Gutierrez, D.: Cross-stratigraphies from a
636 seismically active mud lens off Peru indicate horizontal extensions of laminae, missing
637 sequences, and a need for multiple cores for high resolution records, *Mar. Geol.*, 357, 72–89,
638 doi:10.1016/j.margeo.2014.07.008, 2014a.

639 Salvattecì, R., Gutierrez, D., Field, D., Sifeddine, A., Ortlieb, L., Bouloubassi, I., Boussafir, M.,
640 Boucher, H. and Cetin, F.: The response of the Peruvian Upwelling Ecosystem to centennial-
641 scale global change during the last two millennia, *Clim. Past*, 10(1), 1–17, doi:10.5194/cp-10-1-
642 2014, 2014b.

643 Salvattecì, R., Gutierrez, D., Sifeddine, A., Ortlieb, L., Druffel, E., Boussafir, M. and Schneider,
644 R.: Centennial to millennial-scale changes in oxygenation and productivity in the Eastern
645 Tropical South Pacific during the last 25,000 years, *Quat. Sci. Rev.*, 131, 102–117,
646 doi:10.1016/j.quascirev.2015.10.044, 2016.

- 647 Saukel, C., Lamy, F., Stuut, J. B. W., Tiedemann, R. and Vogt, C.: Distribution and provenance
648 of wind-blown SE Pacific surface sediments, *Mar. Geol.*, 280(1-4), 130–142,
649 doi:10.1016/j.margeo.2010.12.006, 2011.
- 650 Scheidegger, K. F. and Krissek, L. A.: Dispersal and deposition of eolian and fluvial sediments
651 off Peru and northern Chile., *Geol. Soc. Am. Bull.*, 93(2), 150–162, doi:10.1130/0016-
652 7606(1982)93<150:DADDOEA>2.0.CO;2, 1982.
- 653 Schweigger, E.: *El litoral peruano (Segunda edición)*., Lima: Universidad Nacional “Federico
654 Villarreal”, 1964., 1984.
- 655 Sears, M.: Notes on the Peruvian coastal current. 1. An introduction to the ecology of Pisco
656 Bay, *Deep Sea Res.*, 1(3), 141–169, doi:10.1016/0146-6313(54)90045-3, 1954.
- 657 Shao, Y., Ishizuka, M., Mikami, M. and Leys, J. F.: Parameterization of size-resolved dust
658 emission and validation with measurements, *J. Geophys. Res. Atmos.*, 116(January), 1–19,
659 doi:10.1029/2010JD014527, 2011.
- 660 Shao, Y. and Lu, H.: A simple expression for wind erosion threshold friction velocity, *J.*
661 *Geophys. Res.*, 105(d), 22437, doi:10.1029/2000JD900304, 2000.
- 662 Sifeddine, A., Gutiérrez, D., Ortlieb, L., Boucher, H., Velazco, F., Field, D., Vargas, G.,
663 Boussafir, M., Salvatelli, R., Ferreira, V., García, M., Valdés, J., Caquineau, S., Mandeng
664 Yogo, M., Cetin, F., Solis, J., Soler, P. and Baumgartner, T.: Laminated sediments from the
665 central Peruvian continental slope: A 500 year record of upwelling system productivity,
666 terrestrial runoff and redox conditions, *Prog. Oceanogr.*, 79(2-4), 190–197,
667 doi:10.1016/j.pocean.2008.10.024, 2008.
- 668 Smith, R. L.: Circulation patterns in upwelling regimes, *Coast. upwelling*, 13–35, 1983.
- 669 Strub, P. T., Mesías, J. M. J. M., Montecino, V., Rutllant, J. A., Salinas, S., Robinson, A. R. and
670 Brink, K. H.: Coastal ocean circulation off western South America, in *The Sea*, vol. 11, pp.
671 273–313., 1998.
- 672 Stuut, J. W., Prins, M. A. and Weltje, G. J.: The palaeoclimatic record provided by aeolian dust
673 in the deep sea: proxies and problems, *Geophys. Res. Abstr.*, 7, 10886, doi:1607-
674 7962/gra/EGU05-A-10886, 2005.
- 675 Stuut, J.-B. W., Kasten, S., Lamy, F. and Hebbeln, D.: Sources and modes of terrigenous
676 sediment input to the Chilean continental slope, *Quat. Int.*, 161(1), 67–76,
677 doi:10.1016/j.quaint.2006.10.041, 2007.
- 678 Stuut, J.-B. W. and Lamy, F.: Climate variability at the southern boundaries of the Namib
679 (southwestern Africa) and Atacama (northern Chile) coastal deserts during the last 120,000 yr,
680 *Quat. Res.*, 62(3), 301–309, doi:10.1016/j.yqres.2004.08.001, 2004.
- 681 Stuut, J.-B. W., Prins, M. a., Schneider, R. R., Weltje, G. J., Jansen, J. H. F. and Postma, G.: A
682 300-kyr record of aridity and wind strength in southwestern Africa: inferences from grain-size
683 distributions of sediments on Walvis Ridge, SE Atlantic, *Mar. Geol.*, 180(1-4), 221–233,
684 doi:10.1016/S0025-3227(01)00215-8, 2002.
- 685 Suess, E., Kulm, L. D. and Killingley, J. S.: Coastal upwelling and a history of organic-rich
686 mudstone deposition off Peru, *Geol. Soc. London, Spec. Publ.*, 26(1), 181–197,
687 doi:10.1144/GSL.SP.1987.026.01.11, 1987.
- 688 Sun, D., Bloemendal, J., Rea, D. ., Vandenberghe, J., Jiang, F., An, Z. and Su, R.: Grain-size
689 distribution function of polymodal sediments in hydraulic and aeolian environments, and
690 numerical partitioning of the sedimentary components, *Sediment. Geol.*, 152(3-4), 263–277,
691 doi:10.1016/S0037-0738(02)00082-9, 2002.
- 692 Sydeman, W. J., García-Reyes, M., Schoeman, D. S., Rykaczewski, R. R., Thompson, S. a,
693 Black, B. a and Bograd, S. J.: Climate change and wind intensification in coastal upwelling

- 694 ecosystems., *Science*, 345(6192), 77–80, doi:10.1126/science.1251635, 2014.
- 695 Timmermann, A., Okumura, Y., An, S. I., Clement, a., Dong, B., Guilyardi, E., Hu, a.,
696 Jungclaus, J. H., Renold, M., Stocker, T. F., Stouffer, R. J., Sutton, R., Xie, S. P. and Yin, J.:
697 The influence of a weakening of the Atlantic meridional overturning circulation on ENSO, *J.*
698 *Clim.*, 20(19), 4899–4919, doi:10.1175/JCLI4283.1, 2007.
- 699 Unkel, I., Kadereit, A., Mächtle, B., Eitel, B., Kromer, B., Wagner, G. and Wacker, L.: Dating
700 methods and geomorphic evidence of palaeoenvironmental changes at the eastern margin of the
701 South Peruvian coastal desert (14°30'S) before and during the Little Ice Age, *Quat. Int.*, 175(1),
702 3–28, doi:10.1016/j.quaint.2007.03.006, 2007.
- 703 Weltje, G. J.: End-member modeling of compositional data: Numerical-statistical algorithms for
704 solving the explicit mixing problem, *Math. Geol.*, 29(4), 503–549, doi:10.1007/BF02775085,
705 1997.
- 706 Weltje, G. J. and Prins, M. a: Muddled or mixed? Inferring palaeoclimate from size distributions
707 of deep-sea clastics, *Sediment. Geol.*, 162(1-2), 39–62, doi:10.1016/S0037-0738(03)00235-5,
708 2003.
- 709 Weltje, G. J. and Prins, M. a.: Genetically meaningful decomposition of grain-size distributions,
710 *Sediment. Geol.*, 202(3), 409–424, doi:10.1016/j.sedgeo.2007.03.007, 2007.
- 711 Wentworth, C. K.: A Scale of Grade and Class Terms for Clastic Sediments, *J. Geol.*, 30(5),
712 377–392, doi:10.1086/622910, 1922.
- 713

714 Table 1: Averaged parameters (geometric mean diameter (Gmd), amplitude (A) and geometric standard deviation (Gsd)) of the 4 log-normal modes
715 (components) identified from measured size distributions of sediment samples (B6 and G10 cores).

716

717

718

719

720

721

722

723

724

725

726

727

728

729

M1			M2			M3			M4		
Gmd (μm)	A (%)	Gsd	Gmd (μm)	A (%)	Gsd	Gmd (μm)	A (%)	Gsd	Gmd (μm)	A (%)	Gsd
3 ± 1	16 ± 7	1.9 ± 0.2	10 ± 2	43 ± 15	1.9 ± 0.2	54 ± 12	20 ± 10	1.4 ± 0.2	90 ± 13	20 ± 13	1.2 ± 0.2

730 Table 2. Minimum, maximum and average values of the grain size components in each climate unit obtained along the record in the Pisco continental shelf.

731

732

733

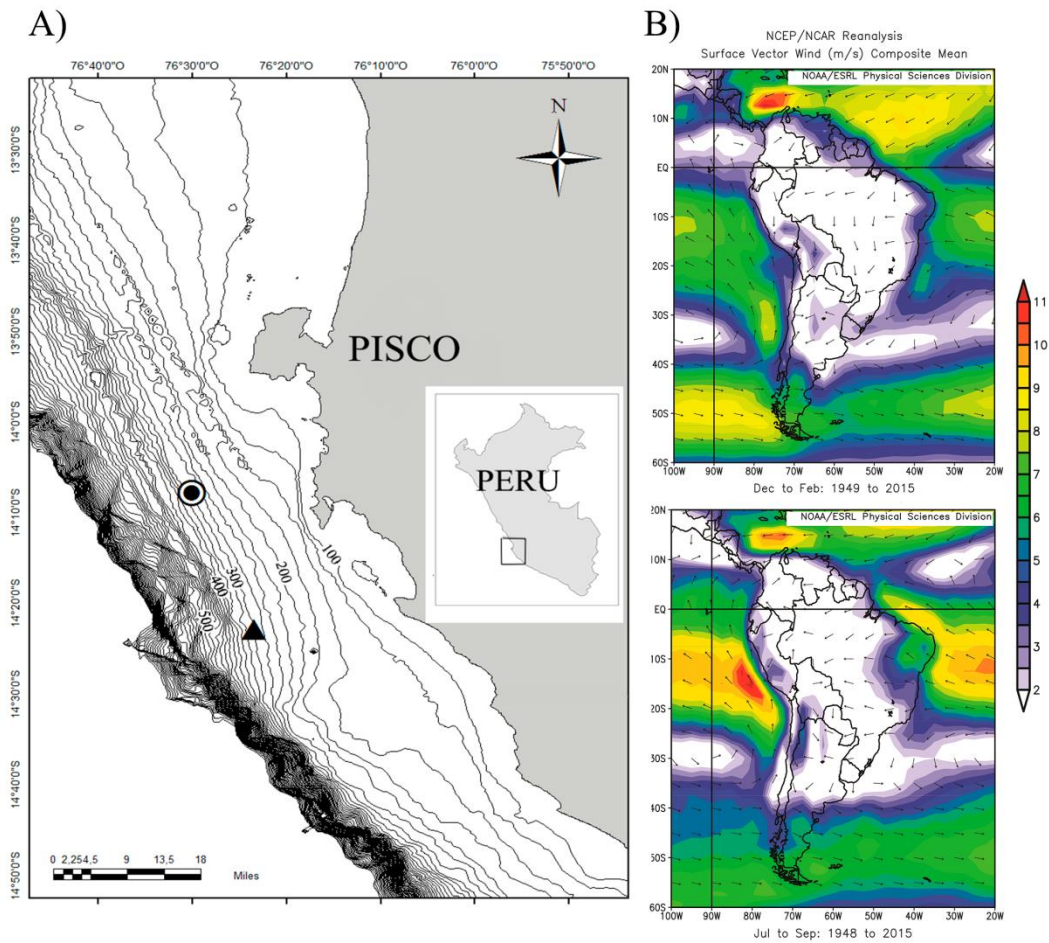
734

735

736

737

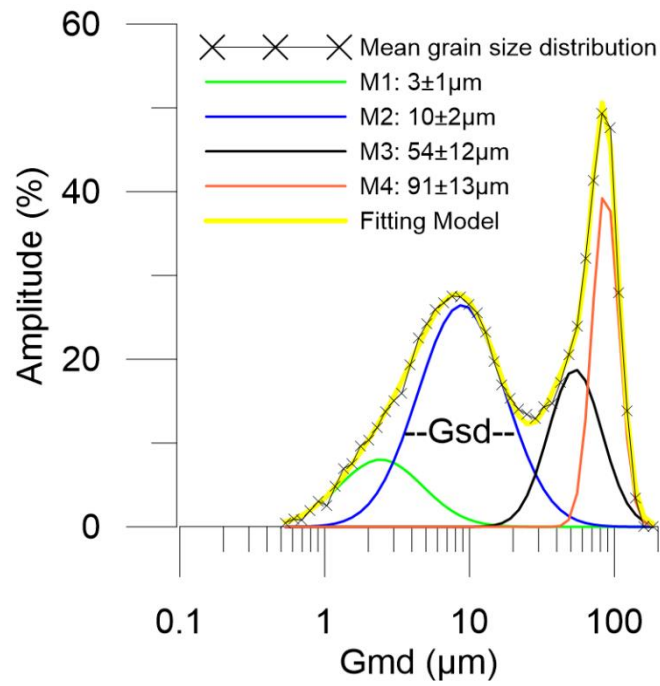
	First period MCA		Second period MCA		LIA		CWP	
	1050 – 1170 A.D.		1170 – 1450A.D.		1450 – 1800 A.D.		1900 A.D to present	
Grain size components	Amplitude (%)		Amplitude (%)		Amplitude (%)		Amplitude (%)	
	Av/Std.Dv.	Range (Min.-Max.)	Av/Std.Dv	Range (Min.-Max.)	Av/Std.Dv.	Range (Min.-Max.)	Av/Std.Dv.	Range (Min.-Max.)
M1	13 ± 5	8 - 19	14 ± 6	5 - 27	15 ± 6	6 - 29	18 ± 7	4 - 40
M2	50 ± 14	33 - 64	36 ± 8	23 - 60	53 ± 15	16 - 80	34 ± 10	13 - 63
M3	16 ± 8	6 - 28	21 ± 10	0 - 39	19 ± 9	4 - 45	23 ± 10	6 - 44
M4	21 ± 5	12 - 30	29 ± 15	10 - 55	14 ± 11	0 - 44	25 ± 13	0 - 56



738

739 Figure 1. A) Location of the sampling of the sediment cores B040506 (black circle) and
 740 G10-GC-01 (black triangle) in the Central Peru continental margin. Bathymetric contour
 741 lines are in 25m intervals from 100m to 500 m depth. B) Mean surface vector wind
 742 velocity (m/s) composite mean for summer (up) and winter (down) between 1948 and
 743 2015 at South American. NCEP/NCAR Reanalysis data.

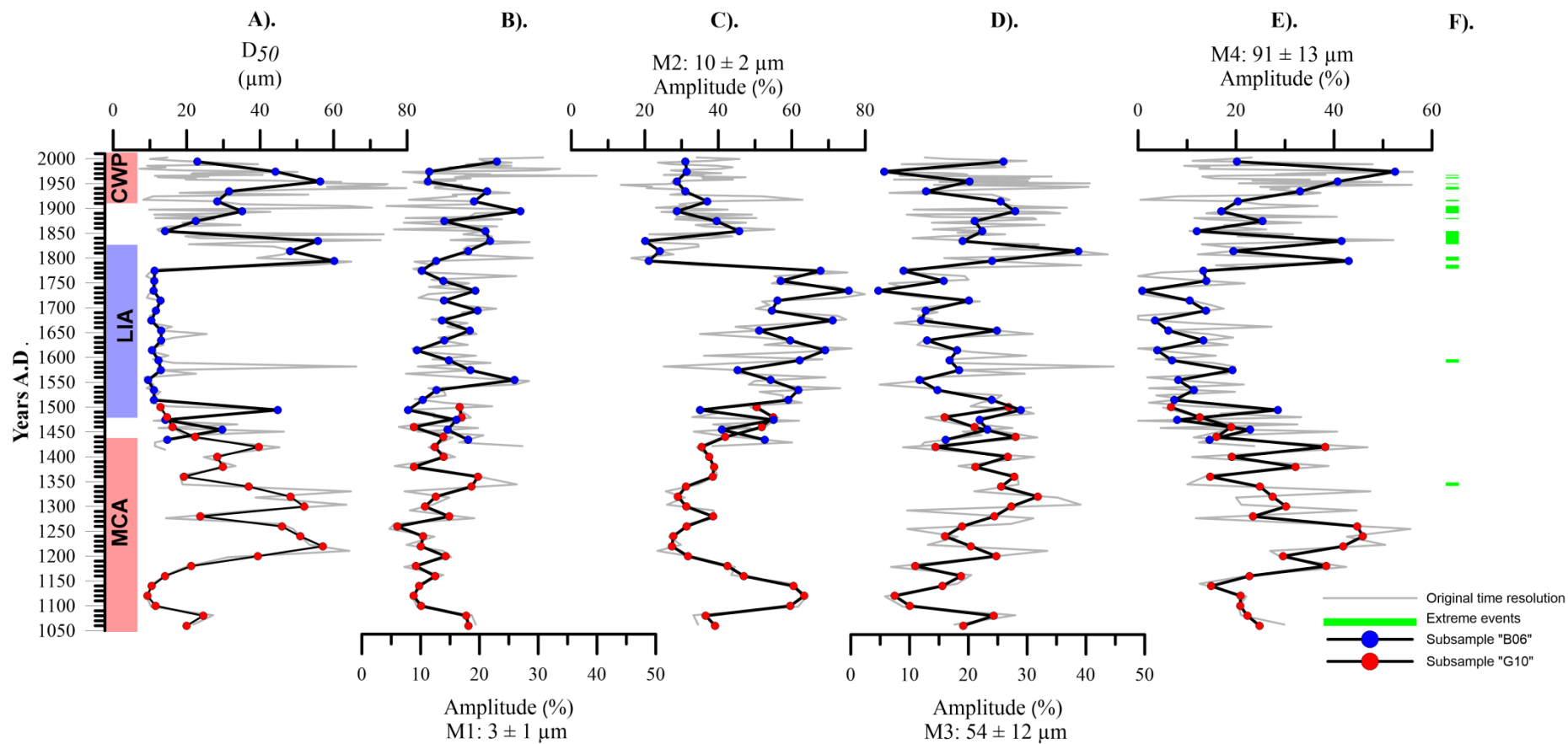
744



745

746 Figure 2: Comparison between a measured grain size distribution and the fitted curve using log-
747 normal function and its partitioning into four individual grain size modes. The measured data is
748 a mean grain-size distribution from all samples of B6 and G10 cores.

749 .



750

751 Figure 3. A) Median grain size (D50) variation along the record and variation in relative abundance of the sedimentary components: B) M1, C) Fluvial (M2),
 752 D) Aeolian (M3) and E) Aeolian (M4) of the grain size distribution in the record. F) Represent the samples where was found very large particles related to
 753 extreme events.

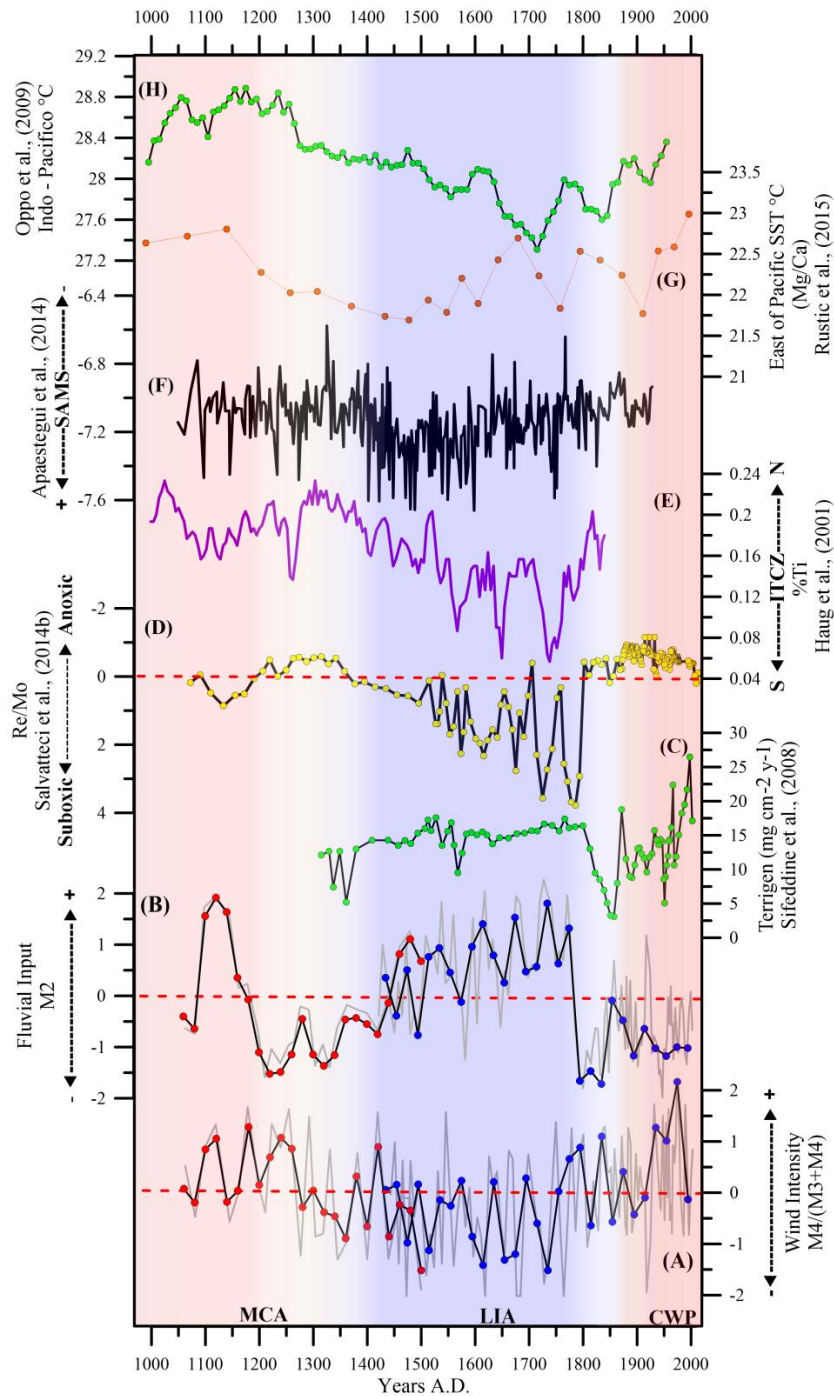


Figure 4. A) Wind intensity ($M4/(M3+M4)$) anomaly reconstruction, B) Fluvial input ($M2$) anomaly reconstruction on the continental shelf, and records of C) Terrigenous flux (total minerals) in Pisco continental shelf by Sifeddine et al (2008), D) OMZ activity (Re/Mo anomalies) negative values indicate more anoxic conditions (the axis was reversed) (Salvatteci et al., 2014b), E) ITCZ migration ($\%Ti$) (Peterson and Haug, 2006), F) SAMS activity reconstruction ($\delta^{18}O$ Palestina Cave) (Apaéstegui et al., 2014), G) Eastern temperatures reconstruction (Rustic et al., 2015) H) Indo-Pacific temperatures reconstruction (Oppo et al., 2009).